Flow Measurement and Instrumentation 27 (2012) 53–58

Contents lists available at SciVerse ScienceDirect

Flow Measurement and Instrumentation

journal homepage: www.elsevier.com/locate/flowmeasinst

Landweber iterative algorithm based on regularization in electromagnetic tomography for multiphase flow measurement

Ze Liu *, Guoyin Yang, Nan He, Xiaoying Tan

School of Electronics and Information Engineering, Beijing Jiaotong University, Beijing, 100044, China

ARTICLE INFO

Keywords:
Electromagnetic tomography (EMT)
Regularization
Landweber iteration algorithm
Image reconstruction

ABSTRACT

For multiphase flow that contains conductive or magnetic permeable material, it is possible to use an electromagnetic tomography technique to measure its flow rate and phase density. The main challenge of this kind of measurement is how to improve the image reconstruction quality. In this paper the comparison of linear back project, Landweber iterative and Tikhonov regularization algorithms are studied for an electromagnetic tomography system. Then an improved method of the Landweber iterative is introduced which uses a Tikhonov regularization reconstruction image as the initial iterative value for the iterative. Compared with the original Landweber iterative using a linear back project result as the initial value, this method can improve the quality of the reconstructed image. Moreover, the convergence speed of the iterative can be improved by using this method. The effectiveness of this method is verified by simulation reconstruction.

1. Introduction

Electromagnetic tomography (EMT) is one kind of electrical tomography that is used to image cross-sections of multiphase flow in industrial processes. The sensor of the EMT system can generate an alternating magnetic field by excitation coils that apply an alternating current. Then the detectors mounted around the measured pipe circle can detect the boundary magnetic flux density [1]. The sensor of EMT has the advantages of being non-invasive, non-contacting and non-hazardous, so the EMT technology can be used in multiphase flow measurement in the industrial area of metallurgical process measurement, chemical abstraction, foreign material monitoring and mineral transporting [2–5].

Many factors are related to the quality of reconstructed image in an EMT system. The factors include excitation field style, excitation frequency, magnetic detectors' structure, measurement signal demodulation and the image reconstruction algorithm. Among these factors, the reconstruction algorithm is critical. Many reconstruction algorithms have been reported in an electrical tomography system including linear back-projection (LBP), the Tikhonov regularization algorithm, Landweber iteration, Newton–Raphson iterative, Tikhonov iterative, algebraic reconstruction algorithm, simultaneous iterative reconstruction and model-based reconstruction algorithm etc. [6–9]. For an EMT system, the LBP algorithm is the basic algorithm, and the Tikhonov regularization and Landweber iterative are widely used in the EMT study for its effectiveness and convenience. Based on the comparison of these algorithms this paper introduces a modified method from the Landweber iterative algorithm for the EMT system. The main improvement of this method is that Tikhonov reconstruction image is used as the initial iterative value. To verify this method, image reconstructions are simulated in a parallel excitation EMT system model.

2. Forward problem of EMT system

The sensor of a typical EMT system includes excitation coils and detector coils. There are two kinds of typical EMT system according to the difference of its excitation coils' geometry and distribution [2]. In this paper, the simulation is based on the parallel excitation structure shown as Fig. 1. The reason to select a parallel model is that the excitation field is parallel and uniform compared with single coil excitation. As shown in Fig. 1 there are four layers in the sensor, which are the pipe wall layer, detection layer, excitation layer and electromagnetic shielding layer. In the excitation layer there are 16 copper strips installed vertically to the cross section of the pipe. When the alternating current is applied to the strips according to sine wave distribution simultaneously, a parallel excitation field can be generated in the pipe [2]. By rotating the distribution of excitation current, the excitation projection can be rotated electrically [10].

In Fig. 1, R_p is the radius of pipe, which is 24 mm. R_e is the radius of the excitation layer, which is 36 mm. R_s is the radius of the shielding layer, which is 52 mm. The simulated flux line distribution of the rotation in the empty pipe condition is as Fig. 2.

* Corresponding author. Tel.: +86 1051684775; fax: +86 1051683974.
E-mail addresses: zliu@bjtu.edu.cn, zliu2005@gmail.com (Z. Liu).

0955-5986/$ – see front matter © 2012 Elsevier Ltd. All rights reserved.
doi:10.1016/j.flowmeasinst.2012.04.011

Nomenclature

B	Magnetic flux density, T
H	Magnetic field intensity, A/m
E	Electric field intensity, V/m
D	Electric flux density, C/m^2
A	Magnetic vector potential, Tm
S	Area of pipe cross section, m^2
U	Vector of induced voltage of detectors, V
S	Sensitivity matrix
G	Gray vector of conductivity distribution
α	Landweber iterative parameter
γ	Tikhonov regularization parameter
λ	Eigen value of matrix $\mathbf{S}^T\mathbf{S}$
σ	Conductivity, S/m
ε	Permittivity
μ	Relative permeability.

The figures are flux line distributions of projection 1, 2 and 4 respectively.

As in Fig. 1, the detector coils are mounted on the detection layer, the coils can measure the boundary magnetic flux density that contains the object field information. The induced voltage of detector $\mathbf{U}_d$ can be described as Eq. (1).

$$\mathbf{U}_d = f(\mathbf{B}_e(x,y), \mathbf{B}_o(x,y), \mu, \sigma(x,y)) \quad (x,y) \in S. \tag{1}$$

Here, the analyzed model is based on the cross section S of the measured pipe, $\mathbf{B}_e$ is the excitation magnetic field, and $\mathbf{B}_o$ is the magnetic field generated by the measured objects' eddy current or magnetization effect. $\mathbf{U}_d$ is related to the measured objects' conductivity, permeability and the excitation condition. Although $\mathbf{U}_d$ is sensitive to both conductivity and permeability, in this paper only conductivity distribution reconstruction is considered because the conductive object and permeable object have a contrary effect on the detector coils [10]. Until now, there has been no effective method to decouple these two kinds of effect from the signal of detector coils or reconstructed images.

The excitation magnetic field in the cross section of the EMT sensor can be described as the Maxwell equations (2) if three assumptions are satisfied. (1) The magnetic sensing field can be considered as a two dimensional harmonic field and the magnetic potential vector **A** only has the Z axial part. (2) The object conductivity is linear and isotropic. (3) The magnetic flux density is sinusoidal and can be symbolized by $e^{j\omega t}$, here ω is the excitation frequency [1,2].

$$\begin{cases} \nabla \times \mathbf{H} = \sigma\mathbf{E} + j\omega\varepsilon\mathbf{E} \\ \nabla \times \mathbf{E} = -j\omega\mathbf{B} \\ \nabla \cdot \mathbf{B} = 0 \\ \nabla \cdot \mathbf{D} = 0 \end{cases} \tag{2}$$

where **B** is magnetic flux density, **H** is magnetic field intensity, **E** is electric field intensity, **D** is electric flux density, ε is the permittivity and σ is the electrical conductivity. Because the frequency of the EMT systems is low enough for the displacement current to be ignored, so $j\omega\varepsilon\mathbf{E} = 0$ can be assumed. The magnetic vector potential **A** of the sensitive field can be simplified to Eq. (3).

$$\nabla^2\mathbf{A} = j\omega\mu\sigma\,(x,y)\,\mathbf{A}. \tag{3}$$

In the cylindrical coordinate system shown in Fig. 1, Eq. (3) can be written as Eq. (4)

$$\frac{1}{\rho}\frac{\partial}{\partial\rho}\left(\rho\frac{\partial\mathbf{A}}{\partial\rho}\right) + \frac{1}{\rho^2}\frac{\partial^2\mathbf{A}}{\partial\varphi^2} = j\omega\,\mu\sigma\,(\rho,\varphi)\,\mathbf{A} \tag{4}$$

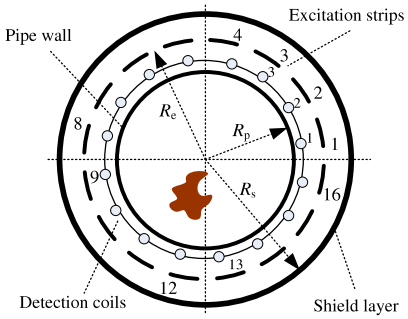

Fig. 1. Cross section of parallel EMT sensor.

where ρ is the radial distance and φ is the angle in the cylindrical coordinate system. After the magnetic vector potential **A** is solved by the finite element method in the measured cross section, the detector coils' induced voltage U_d can be expressed as Eq. (5).

$$U_d = -\frac{d\psi}{dt} = -n\cdot\frac{d(B\cdot S_d)}{dt} = -n\cdot\frac{d(A\cdot l)}{dt}. \tag{5}$$

Here, ψ is the magnetic flux. n, S_d, l represent the detector coil's turn, area and axial length respectively. Then by tuning the projection of excitation magnetic field and acquiring the coils' induced voltage, the result of EMT's forward problem can be obtained.

3. Sensitivity matrix calculation and measurement data simulation

As the prior information of image reconstruction, the sensitivity matrix consists of the relationship between measurement data and test objects in the sensing field. In an EMT system, sensitivity matrix $\boldsymbol{S}$ can be used to denote the maps of a particular detector to a small perturbation of one test element area in each projection. In this paper, the sensitivity matrix is calculated by using the electromagnetic module of finite element method software ANSYS. The simulation script APDL (ANSYS Parametric Design Language) is used to write a program to automatically test conductive objects in the pipe area and solve the result of the magnetic field in discrete format. In the model script, the cross section of the flow pipe is meshed into 828 elements. These elements are used as test objects respectively to calculate the 16 detector coils' induced voltage in 16 projections. So the sensitivity matrix $\boldsymbol{S}$ has the structure of $828 \times 16 \times 16$. The sensitivity of detectors on 828 elements in different projections can be displayed on the meshed pipe area according to the leveled filling color. Fig. 3 shows four sensitivity maps of a total of 256. Where p is the projection number, d is the detector coil number.

The electromagnetic finite element simulation script is also used to generate the detector coils' output value when the sample conductive objects are set in the sensing field for a specific flow pattern. Fig. 4 is the magnetic flux density vector and magnetic field intensity contour distribution when four copper bars, whose radii are 2 mm, are distributed in the pipe. Then measurement data U_d is calculated according the magnetic flux density on the 16 detectors at 16 excitation projections.

4. Modified Landweber iterative algorithm

The EMT inverse problem can be attributed to the solution of the first class of nonlinear Fredholm integral equations as Eq. (6) [4].

$$\mathbf{U}_d = \iint_D f\,(\mu\cdot\sigma\,(x,y))\cdot\mathbf{B}\,[\mu\cdot\sigma\,(x,y)]\,dxdy \tag{6}$$

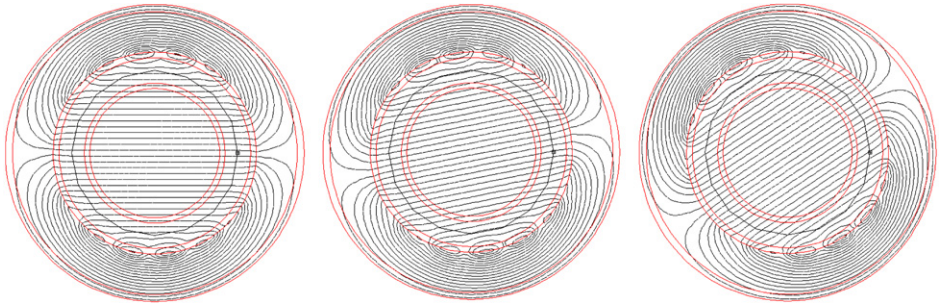

Fig. 2. Flux line distribution of the sensor's cross section.

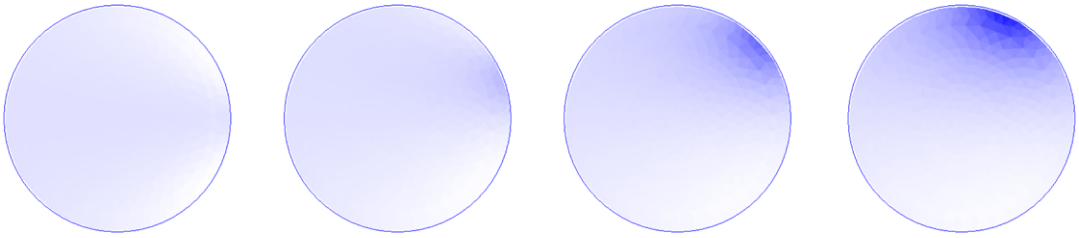

Fig. 3. Sensitivity distribution of the simulation model.

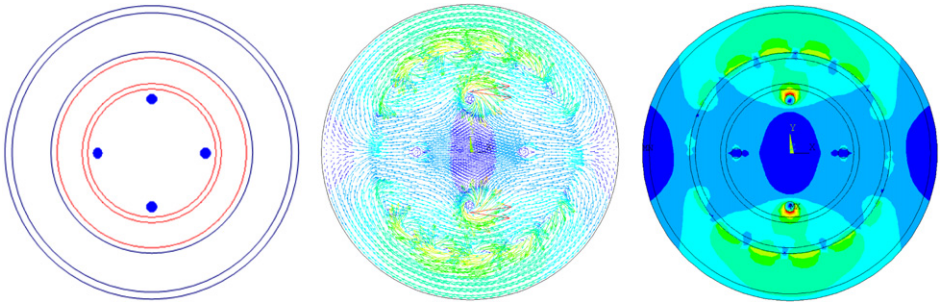

Fig. 4. Magnetic flux density vector and magnetic field intensity contour distribution.

where $f(\mu \cdot \sigma(x, y))$ is the distribution of conductive material in the measured field. **B** is the system characteristic function that is affected by the material distribution. The EMT inverse problem is to seek the solution of the $f(\mu \cdot \sigma(x, y))$ when the $\mathbf{U}_d$ is known as the measured data. With a limited number of measured data and limited elements of material distribution, the equation can be expressed as linear matrix equation Eq. (7).

$$\mathbf{U} = \mathbf{SG}. \tag{7}$$

Here **U** is the column vector of the induced voltage of detectors, and **S** is the sensitivity matrix. **G** is the column vector of gray or the probability of conductivity distribution on each meshed element. The Landweber iterative reconstruction algorithm is as Eq. (8)[6,11].

$$\begin{cases} \mathbf{G}_0 = \mathbf{S}^{\mathbf{T}}\mathbf{U} & \text{(a)} \\ \mathbf{G}_{k+1} = \mathbf{G}_k + \alpha \mathbf{S}^{\mathbf{T}}(\mathbf{U} - \mathbf{SG}_k) & \text{(b)} \end{cases} \tag{8}$$

where, $\mathbf{G}_0$ is the initial value of the iterative, **U** is the induced voltage vector, $\mathbf{G}_0$ is calculated by using the LBP algorithm, k is the iteration step number, and α is an iterative parameter which is used to control the convergence speed.

Image reconstruction simulation shows that the reconstruction image using Eq. (8) is affected by the initial value G_0. The quality of the iterative image is hard to improve when the quality of G_0 is weak. So improving the quality of the initial reconstructed image is a possible way to enhance the final iterative quality. For the direct reconstruction algorithm, Tikhonov regularization is more accurate than that of LBP. Tikhonov regularization is a derivate method of parameter identification by using the regularized least square method. It can solve the EMT's ill-posed problem by adding a scaling identity matrix [4]. So in this paper the Landweber iterative regularization is used as the initial iterative value special for EMT. This kind of modification was also tested in ECT (electrical capacitance tomography) as [12] reported. After changing the initial value, the Landweber iterative algorithm becomes Eq. (9).

$$\begin{cases} \mathbf{G}_0 = \left(\mathbf{S}^T\mathbf{S} + \gamma\mathbf{I}\right)^{-1}\mathbf{S}^T\mathbf{U} & \text{(a)} \\ \mathbf{G}_{k+1} = \mathbf{G}_k + \alpha\mathbf{S}^T(\mathbf{U} - \mathbf{SG}_k) & \text{(b)} \end{cases} \tag{9}$$

where, γ is the regularization parameter. **S** is the sensitivity matrix. By adding a unit matrix with a factor γ the Tikhonov regularization algorithm can make the $\mathbf{S}^T\mathbf{S}$ matrix generalized inverse to enhance the reconstructed image. After replacing the Landweber algorithm's initial value, the iterative stable convergence criterion still satisfies Eq. (10), which is studied in [6], because the convergence is only affected by the image correction part of the iterative equation.

$$\left\|\alpha\mathbf{S}^T\mathbf{S}\right\|_2 < 2. \tag{10}$$

Suppose $\lambda_{\max}$ is the maximum eigen value of $\mathbf{S}^T\mathbf{S}$, the gain factor α should be in the following range to maintain the iterative algorithm's convergence.

$$0 < \alpha < 2/\lambda_{\max}. \tag{11}$$

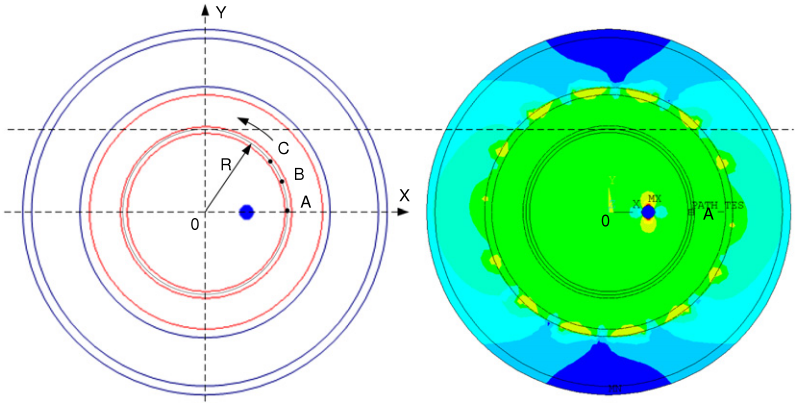

Fig. 5. Magnetic flux density distribution of a test copper bar in the pipe.

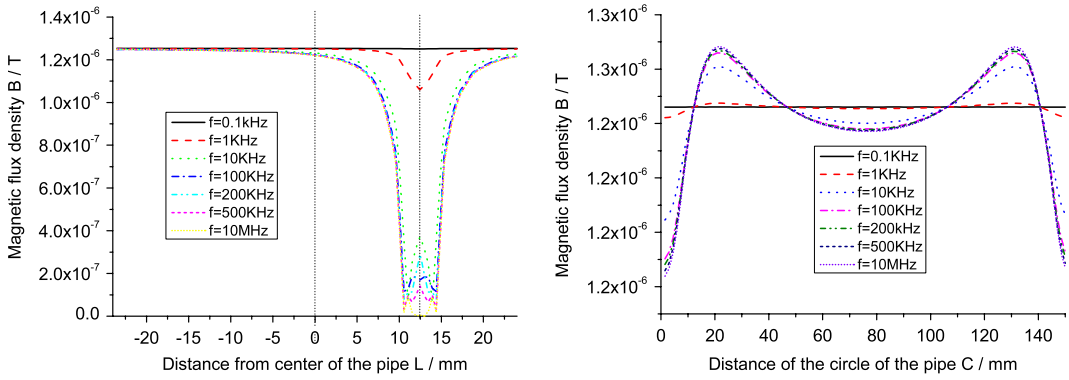

(a) Along X-axes. (b) Along test circle path.

Fig. 6. Magnetic flux density distribution in difference frequency.

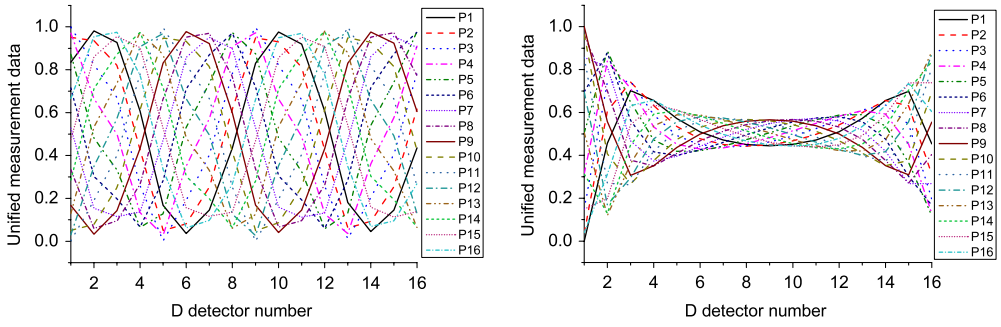

(a) Empty field. (b) Object field with copper bar.

Fig. 7. Measurement data of 16 detectors in 16 directions.

5. Image reconstruction simulation

Image reconstruction using the modified Landweber iterative algorithm is tested by reconstruction simulation in the following condition. The simulation is based on the parallel model as Fig. 1. The frequency of the forward problem solution is 100 KHz. The maximum excitation current on the strips is 10 mA. The excitation frequency optimization of the model is verified by simulation. When a copper bar is placed in the pipe its induced eddy current will change according to the excitation frequency. Fig. 5 is the model where a radius 2 mm copper bar is placed in the right center of the pipe. Fig. 6 is the magnetic flux density distribution along the X-axial and a test circle path in a different excitation frequency. The simulated frequency is from 0.1 KHz to 10 MHz. The test circle path is as shown in Fig. 5 left. The radius R of the test circle path is 24 mm and the starting point of the path is point A where $x = 24$ and $y = 0$ mm. The rotation direction is anticlockwise. As shown in Fig. 6, when the excitation frequency is larger than 100 KHz, the magnetic flux density induced by eddy current in the copper object is not obviously increasing. Therefore, around 100 KHz is an economical and sufficient excitation frequency range for an EMT sensor with this structure.

In all 16 projections the measurement data with empty field and with the test 2 mm radius copper bar are shown as Fig. 7(a) and (b) respectively. In the empty field, the unified measurement data is similar in shape in different projections. Nevertheless, when the copper bar is in the pipe, the closer the detector is from the copper bar, the greater the influence on the measurement data from the eddy current induced in the bar.

Based on the model, the image reconstruction simulation has been done with LBP, Landweber iterative, Tikhonov regularization and modified Landweber iterative algorithms. The simulation

Table 1
Simulated image reconstruction result.

No.	Flow pattern	LBP (Eq. (7))	Landweber (Eq. (8), $\alpha = 0.0039$, $k = 10$)	Tikhonov regularization (Eq. (9)a, $\gamma = 0.1$)	Modified Landweber (Eq. (9), $\gamma = 0.1$, $\alpha = 0.0039$, $\Delta g \leq 0.1$)	k_s	Modified Landweber (Eq. (9), $\gamma = 0.1$, $\alpha = 0.0039$, $\Delta g \leq 0.01$)	k_s
1						4		18
2						5		19
3						5		17
4						5		17
5						4		24
6						1		11

result is as shown in Table 1. There are six typical flow patterns in the table. The reconstruction result of different algorithms with specific parameters is shown in the columns. The reconstruction result is affected by the regularization parameter γ and the iterative parameter α. In Table 1, the images are reconstructed based on the pre-optimized parameters γ and α.

As shown in Table 1, in the LBP column the reconstruction result cannot identify the position of test objects, especially when there are multiple ones. In the Landweber iterative column, the algorithm cannot improve the quality of the reconstructed image obviously compared with LBP. The simulated measurement data, sensitivity matrix and algorithm programming are checked carefully for the Landweber column. In addition, a different iterative parameter α is also tested. The Landweber result is still not ideal. In the Tikhonov regularization column, the quality of reconstructed images is obviously improved. For the modified Landweber iterative algorithm, there are two columns. The difference between these two columns is that the iterative stop condition parameter Δg is different. Δg is defined as Eq. (12). And K_s in the table are the iterative times when the iterative is stopped.

$$\Delta g = \sum_{e=1}^{N} \left|\mathbf{G}_{k+1,e} - \mathbf{G}_{k,e}\right| \Big/ \sum_{e=1}^{N} \left|\mathbf{G}_{k,e}\right| \tag{12}$$

where e is the meshed element number in the pipe, N is the total element number, which is 828. $G_{k,e}$ is the gray value of number e element. As shown in the table the iterative times K_s are different with the same iterative stop condition in different flow patterns. Δg is the image correction value of the iterative process. The Δg's change in different patterns with the condition of $\Delta g \leq 0.01$ is shown in Fig. 8.

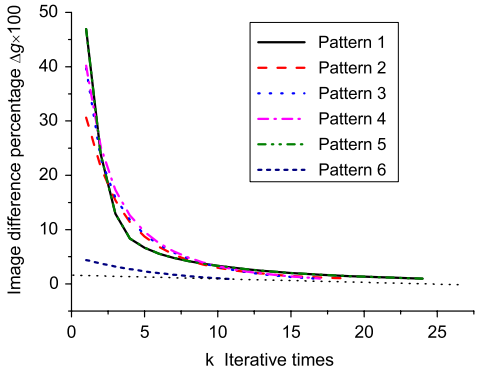

Fig. 8. Δg's change in different patterns with the condition of $\Delta g \leq 0.01$.

As shown in Fig. 8, the iterative process is convergent with the condition. Moreover, the image quality of the modified Landweber iterative is improved compared with the initial Landweber iterative in the EMT system.

6. Conclusion and discussion

LBP, Landweber iterative and Tikhonov regularization reconstruction algorithms are simulated in a parallel excitation EMT system model for multiphase flow measurement. Based on the comparison, a kind of modified Landweber iterative algorithm is introduced, which uses Tikhonov regularization reconstruction as the initial iterative value. Simulation in six typical patterns verified the performance of the modified iterative algorithm. Future

work will focus on the evaluation of magnetic permeable material reconstruction. Moreover, the performance comparison of parallel excitation and single coil excitation at a similar sensor structure will be studied.

Acknowledgment

The authors acknowledge the support of the National Natural Science Foundation of China (NSFC, grant No. 61050001).

References

[1] Yu ZZ, Peyton AT, Beck MS, Conway WF, Xu LA. Imaging system based on electromagnetic tomography (EMT). Electron Lett 1993;29:625–6.
[2] Peyton AJ, Yu ZZ, Lyon G, Al-Zeibak S, Ferreira J, et al. Overview of electromagnetic inductance tomography: description of three different systems. Meas Sci Technol 1996;7:261–71.
[3] Terzija Natasa, Yin Wuliang, Gerbeth Gunter, Stefani Frank, Timmel Klaus, Wondrak Thomas, Peyton Anthony. Electromagnetic inspection of a two-phase flow of GaInSn and argon. Flow Meas Instrum 2011;22:10–6.
[4] Yin W, Peyton AJ, Stefani F, Gerbeth G. Theoretical and numerical approaches to the forward problem and sensitivity calculation of a novel contactless inductive flow tomography (CIFT). Meas Sci Technol 2009;20:10–3.
[5] Ismail I, Gamio JC, Bukhari SFA, Yang WQ. Tomography for multi-phase flow measurement in the oil industry. Flow Meas Instrum 2005;16:145–55.
[6] Yang WQ, Peng Lihui. Image reconstruction algorithms for electrical capacitance tomography. Meas Sci Technol 2003;14:R1–13.
[7] Liu S, Fu L, Yang WQ. Optimization of an iterative image reconstruction algorithm for electrical capacitance tomography. Meas Sci Technol 1999;10:37–9.
[8] Wang M. Inverse solutions for electrical impedance tomography based on conjugate gradients methods. Meas Sci Technol 2002;13:101–17.
[9] Wang Huaxiang, Wang Chao, Yin Wuliang. A pre-iteration method for the inverse problem in electrical impedance tomography. IEEE Trans Instrum Meas 2004;53(4):1093–6.
[10] Liu Ze, He Min, Xiong Hanliang. Simulation study of the sensing field in electromagnetic tomography for two-phase flow measurement. Flow Meas Instrum 2005;16:199–204.
[11] Yang WQ, Spink DM, York TA, McCann H. An image-reconstruction algorithm based on Landweber's iteration method for electrical-capacitance tomography. Meas Sci Technol 1999;10:1065–9.
[12] Chen Zhikun, Zhao Bo, Wang Hongyan. New Landweber method based Tikhonov for image reconstruction for ECT. Electron Meas Tech 2007;30:61–4.